Saliency Guided Computer-aided Diagnosis for Neurodegenerative Dementia

Olfa Ben Ahmed[1], Mohamed-Chacker Larabi[1], Marc Paccalin[2] and Christine Fernandez-Maloigne[1,*]
[1]*XLIM-SIC, UMR CNRS 7252, Bvd Marie and Pierre Curie, 86962 Futuroscope Chasseneuil Cedex, France*
[2]*Université de Poitiers, Pôle de Gériatrie, CMRR, CHU La Miltrie 86021 Poitiers, EA3808, Poitiers, France*

Keywords: Alzheimer's Disease, Saliency Maps, Visual Attention, Machine Learning, MRI, Domain Knowledge.

Abstract: Visual assessment of brain atrophy for brain diseases diagnosis by clinicians is the most widely adopted method in clinical practices. Such a visually extracted knowledge represents a great potential to develop better training programs and create new tools to assist clinical decision making. Inspired by the clinician visual behavior, we propose in this work a new and automatic approach to detect and quantify local brain atrophies. The proposed approach combines both bottom-up and top-down visual saliency using domain knowledge in the brain MRI analysis. The first subsystem relies on low-level MRI characterization (texture and edge) while the second is based on an embedded learning process to identify and localize the subset of gray matter regions that provides optimal discrimination between subjects. The proposed method validated for the task of Alzheimer's disease (AD) subjects recognition. Classification experiments were conducted on a subset of 188 anatomical MR images extracted from the Alzheimer's Disease Neuro-imaging Initiative (ADNI) dataset. We report accuracy of 81.48% and 76.66% respectively for AD versus Normal Control (NC) and Mild Cognitive Impairment (MCI) versus NC classification tasks.

1 INTRODUCTION

Alzheimer's disease (AD) is a neurodegenerative disease associated with the loss of memory and deterioration in cognitive functions. To date, AD diagnosis is most widely performed based on the visual assessment of brain atrophy (Harper et al., 2016), which is very difficult, tedious and time consuming task. The development of an automated approach for objective visual interpretation of MRI content could potentially increase the visual assessment skills of radiologists by stressing some overlooked image features that may be relevant to the diagnostic problem. This also could make the diagnosis easier for clinicians with a limited expertise in order to extract diagnostically useful and objective information. Hence, modeling the experts' knowledge and perceptual expertise helps to improve structural abnormalities detection and then assists clinicians in the diagnostic task (Li et al., 2013) (Lala and Nakazawa, 2016).

To that end, saliency modeling has been widely explored to describe the radiologists' visual attention for Computer Aided Diagnosis (CAD) (Wen et al., 2016). Saliency-based methods, aiming at detecting lesions and tissue abnormalities, recently attracted more and more attentions and achieved promising results in tumor detection. For instance, (Mehmood et al., 2013b) proposed a prioritization based approach to help clinicians to quickly determine and access the required level of visual information of a particular brain tumor case from brain MRI. In (Nodine and Kundel, 1987), the authors proposed a model for tumor detection in chest X-ray images. They collected the eye tracking data of radiologists, while analysing images in presence of abnormalities, to develop a model for predicting the sequence of events from the time of viewing X-ray images up to the diagnostic decision-making. For a different task, Chung et al. (Chung et al., 2015) proposed a novel saliency-based method for identifying suspicious regions in multi-parametric MR prostate images based on statistical texture distinctiveness. (Banerjee et al., 2016) proposed a saliency detection model to automatically detect and isolate the tumor region from multi-channel brain MRI. Moreover, visual saliency models have been proposed for retinal images analysis. For instance, Deepak et al. proposed a visual saliency-based framework for detecting potential lo-

*For the Alzheimer's Disease Neuroimaging Initiative.

Ben Ahmed O., Larabi M., Paccalin M. and Fernandez-Maloigne C.
Saliency Guided Computer-aided Diagnosis for Neurodegenerative Dementia.
DOI: 10.5220/0006293001400147
In *Proceedings of the 10th International Joint Conference on Biomedical Engineering Systems and Technologies (BIOSTEC 2017)*, pages 140-147
ISBN: 978-989-758-215-8

cations of abnormalities in retinal images (Deepak et al., 2013). Lesions are detected based on their saliency values and local binary pattern features using a k-NN classifier. In the same vain, Zou et al proposed a learning-based visual saliency model method for detecting diagnostic diabetic macular edema regions of interest (ROIs) in retinal images (Zou et al., 2016). Others saliency-based solutions have shown promising results in ROI segmentation and lesion detection for various diseases. For instance, in (Agrawal et al., 2014), a novel framework is developed to automatically detect masses from mammograms even in the presence of regions of pectoral muscles. The framework uses a saliency-based segmentation and features extraction for mass description. With the aim to investigate the relevance of computational saliency models in medical images and the context of lesion detection in chest X-ray images, Jampani et al. conducted the work described in (Jampani et al., 2012). Another automatic segmentation method of ROIs in MRI using saliency information has been proposed by Mehmood et al. (Mehmood et al., 2013a) together with the use of active contours. A graph knowledge-based approach for internal brain structures recognition and internal brain structures segmentation from 3D MRI has been introduced in (Fouquier et al., 2012). Mahapatra et al. (Mahapatra and Buhmann, 2015) proposed a new approach for MRI prostate segmentation using active learning and visual saliency. In (Yuan et al., 2015), the authors proposed a visual saliency-based computer-aided detection system to detect ulcers from wireless capsule endoscopy images for human digestive tract diagnosis. The proposed saliency method is based on multi-level super-pixel color and texture representation. In (Shao et al., 2015), the authors modulated the radiologist's visual attention from breast ultrasound (BUS) images to automatically locate suspicious lesions. Automatic extraction and interpretation method of focus tissues from Computerized Tomography (CT) liver images using a visual attention model is proposed in (Ma et al., 2009). The latter firstly extracts texture features of liver regions form Gaussian pyramid of feature-component maps and the saliency map is then generated by combining several conspicuity maps. Finally, ROI candidates are located by labeling the obtained saliency map.

Recently, visual saliency models have been used to model group difference in structural brain MRI for neurodegenerative disease detection such as for AD. In (Pulidoa et al., ; Pulido et al., 2013), the authors extract relevant information from brain MRI using a regional saliency method. They perform classification of brain MR images, based on finding pathology-related patterns through the identification of regional structural changes, associated or not, to the presence of probable AD or Mild Cognitive Impairment (MCI). Rueda et al. proposed an automatic image analysis method based on saliency maps for group diagnosis (Rueda et al., 2014). The graph-based visual saliency (GBVS) algorithm (Harel et al., 2006) is used to generate saliency maps to highlight particular regions.

In the aforementioned works, authors do not include any domain knowledge information regarding AD which makes the model weak for specific AD diagnosis tasks. They also straightforwardly use traditional and multimedia oriented saliency algorithms without accounting for MRI images properties in the AD diagnosis context. In addition, the used saliency maps and kernel matrices require extensive computations. Those works are proposed for the group analysis study and they have no value at the individual level. Contrariwise, we propose in this paper a novel saliency model adapted to AD diagnosis from MRI content interpretation at the individual level. The proposed approach extracts, spots and describes ROIs in the structural MRI images offering thus an assistance to clinician in the AD diagnosis making stage. The proposed model combines bottom-up and top-down approaches using domain knowledge in AD diagnosis. The first part benefits from the low level MRI characterization (texture and edge) while the second is based on an embedded learning process to identify and rank discriminative regions for AD diagnosis. The rest of the paper is organized as follows, section 2 is dedicated to the detailed description of the proposed approach. Simulation results and discussions are given in Section 3. Finally, Section 4 concludes the paper and gives some openings for future work.

2 PROPOSED APPROACH

This section aims at presenting the proposed approach to build the visual saliency maps for ROI detection in the case of AD diagnosis. The proposed approach is based on a combination of two subsystems : 1) the bottom-up part corresponding to image features and 2) the top-down part relying on the knowledge and expertise of radiologists in AD diagnosis. Figure 1 illustrated the pipeline of the proposed method highlighting the two subsystems mentioned above.

The bottom-up saliency map is computed using edge and texture characteristics of the MRI images while the top-down map is obtained by ranking from MRI the effectiveness of the gray matter (GM) brain regions to discriminate healthy brains from those affected by AD using a machine learning strategy. The final saliency map results from the fusion of the

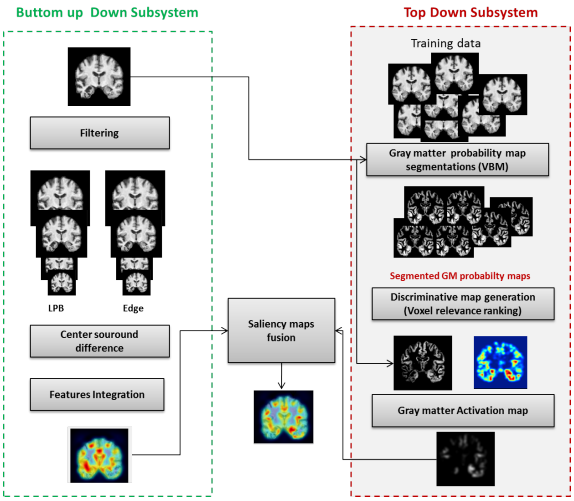

Figure 1: Pipeline of the proposed AD saliency map generation combining both bottom-up and top-down strategies.

saliency maps obtained respectively from the top-down and bottom-up subsystems.

2.1 Domain Knowledge and Hypothesis Generation in MRI Visual Assessment

From a practical point of view, a clinician with some expertise may be able to identify the most atrophic brain areas on a given MRI image. This result is achieved by looking for structural brain variations. According to (Braak and Braak, 1998), the pattern of cell neuro-degeneration seen using anatomical MRI in several brain areas may be considered as sensitive bio-markers for AD. In visual assessment-based MRI analysis, the brain shrinkage could be seen as a variation of tissue properties (i.e. density). In fact, the brain tissue density reflects the amount of tissue present in each subject's image at a given location. For example, a region of decreased density reflects a reduced volume in this structure (increasing medial temporal atrophy, MRI cortical thickness shrivels up, loss of hippocampus volume and ventricular enlargement in AD when compared with Normal Control (NC),etc). In the case of AD, the volume losses generally convey a loss of GM cells (Blennow et al., 2010). This is why neuro-imaging research is mostly focused on this tissue.

2.2 Top-down Saliency Map

Locally shrunk brain structure is seen with different proportion of GM compared to the case where they are unaffected. Such a "top-down" knowledge is incorporated into a saliency map. Therefore, we propose first to build a spatial map of GM tissues using the voxel based morphometry (VBM) method (Ashburner and Friston, 2000). Indeed, each MRI is segmented into three tissues : GM, white matter (WM) and cerebrospinal fluid (CSF). This segmentation is performed using a technique based on a mixture of Gaussian distribution cluster analysis which identifies voxels intensity distribution of a particular brain tissue. The obtained three probability maps contain values in the range of 0 to 1, representing the prior probability of a voxel being either GM, WM or CSF. These spatial maps give a quantitative representation of the spatial distribution of tissues in the brain, with brightness being proportional to the amount of local tissue volume before warping. The probability of a voxel at $(i; j)$ coordinates belonging to cluster $Class = \{GM, WM, CSF\}$ is denoted by $P((i, j)/Class)$. For example, $P((i, j)/GM)$ is the probability of a voxel being GM.

Once the GM maps are built, we propose to modulate the clinician preference location by the "so-called" ranking map (Rank-Map). This is the first stage to build the top-down saliency map. We learn whether the brain tissue from AD patients could be differentiated from that of NC in the standard space. Therefore, we developed a recursive feature elimination (RFE) (Guyon et al., 2002) approach to recursively learn relevant regions of GM. Our goal is different from what is usually done to eliminate non relevant features, it consists in ranking and projecting MRI GM voxels according to their contribution in separating AD and NC subjects into a spatial map. The ranking criterion is derived from the SVM (Hearst et al., 1998) model.

Subjects Data. For the purpose of this work, we used the ADNI dataset [1]. For the Rank-Map generation, we selected from the ADNI dataset T1-weighted structural MRI, a total of 205 participants with 95 AD patients and 110 NCs. NC subjects aged between 60 and 92 have Mini Mental State Examination (MMSE) scores ranging from 24 to 30 while AD subjects aged between 55 and 91 have MMSE scores ranging from 18 to 27. Groups statistical difference was performed using t-test, the $p - value$ between groups for both MMSE and age is < 0.001.

In our approach, each medical image is first preprocessed by applying for each subject, corrections for eddy currents and head motion, skull stripping with the Brain Extraction Tool (BET) Software Library FSL [2]. Then, the whole set of MR images are

[1] http://adni.loni.ucla.edu/
[2] http://www.fmrib.ox.ac.uk/fsl

co-registered to the Montreal Neurological Institute (MNI) standard space using MNI 512 brain template (Frisoni et al., 2005) thanks to the freely available VBM8 toolbox [3] using statistical parametric mapping (SPM)[4] software running on Matlab. After the preprocessing stage, all MR images have a size of $121 \times 145 \times 121$ voxels having a voxel size of 1.5 mm $\times$1.5 mm $\times$1.5 mm.

Given a training of instance label pairs $(x_i, y_i), i = 1, ..., l$ (l is the number of training data) where $x_i \in R^n$ and $y \in \{1, -1\}$, x_i is the feature vector of in n dimensions that describes the image and y_i is the corresponding label of x_i. SVM searches to find the optimal hyperplane that best separates the positive and negatives training samples. The optimization problem to resolve, in the case of the so-called "soft margin" classification, is the following:

$$\begin{aligned} &minimize_{w,\xi} \quad \frac{1}{2}\|w\|^2 + \frac{C}{l}\sum_{i=1}^{l}\xi_i \\ &subject\,to \quad y_i(w^T x_i + b) \geq 1 - \xi_i, \xi_i \geq 0 \end{aligned} \tag{1}$$

ξ_i are the so-called slack variables relaxing class-separators constraints and C is a cost parameter that controls the trade-off between allowing training errors and forcing rigid margins. RFE was conducted by ranking voxels in terms of magnitude of their weights w where the ranking criterion is $c_i = (w_i)^2$. Larger the absolute magnitude of a weight vector is, stronger it affects the final discrimination. At every iteration, the feature $f = argmin(c)$ will be removed. The SVM then retrains the remaining features to obtain the new feature sorting. SVM-RFE repeatedly implements the process until obtaining a feature sorted list. Because of the multivariate nature of the classifier, the distribution of weights over all voxels can be interpreted as the spatial pattern by which the groups differ (i.e. the discriminating pattern). The SVM-RFE algorithm was embedded within a leave-one-out cross validation (LOO-CV) framework. The average CV accuracy over all subjects for each feature set size has been computed to find the optimal number of features. The percentage of most pertinent voxels is set to 30% corresponding to the best AD *versus* NC classification accuracy as illustrated by Figure 2.

The Rank-Map is obtained by projecting the obtained stored ranked features into the MNI coordinate space $Rank_{map}(x, y)$ in which each pixel is represented by its rank r (more the pixel is relevant more its intensity is higher). This pixel relevance illustrates the clinician preference order in brain areas inspection. The first ranked areas could be the most important for clinician and consequently the first target to examine.

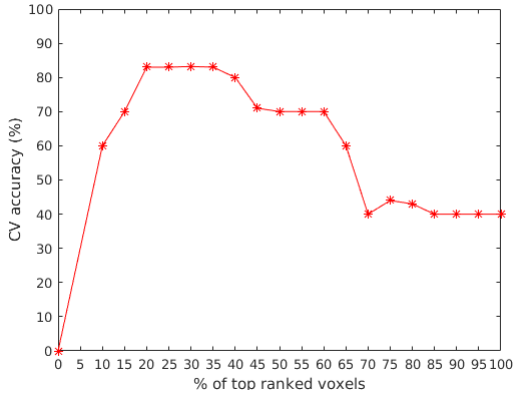

Figure 2: Percentage of top ranked voxels variation over CV accuracy (AD *versus* NC classification).

$$Rank_{map}(x, y) = r, \tag{2}$$

where, (x, y) are the MNI coordinates of r^{th} most important pixel. Finally the Rank-Map is normalized as follows in order to build a ranking image:

$$Rank_{map} = \frac{Rank_{map} - min(Rank_{map})}{max(Rank_{map}) - min(Rank_{map})}. \tag{3}$$

The top-down saliency map is generated for each subject using the obtained standard Rank-Map. Referring to the domain knowledge, we suppose that the clinician gazes at the most important GM region (regions captured by the normalized Rank-Map) in the GM distribution. Therefore, we compute the top-down saliency map of each subject by conserving only the relevant features that represent non degenerated GM tissues ($P(GM) \geq 0.5$) (Ashburner and Friston, 2000).

$$S_{TP} = \begin{cases} Rank_{map}, & \text{if } P(GM) \geq 0.5). \\ 0, & \text{otherwise.} \end{cases} \tag{4}$$

The obtained top-down saliency map is normalized between 0 to 1 and represents salient pixels for AD diagnosis. All the degenerated GM voxels will be presented by 0 meaning that they are not important for the diagnosis and will be ignored for the visual assessment made by the clinician. The S_{TP} is spatially smoothed using a Gaussian kernel G:

$$S_{TP} = S_{TP} * G \tag{5}$$

2.3 Bottom-up Saliency Map

The image analysis methodology to extract discriminant visual patterns for AD diagnosis is close to visual inspection performed by the clinician. Hence,

[3] http://dbm.neuro.uni-jena.de/vbm/
[4] http://www.fil.ion.ucl.ac.uk/spm/software/

we propose a system based on the Itti model (Itti et al., 1998). Referring to the domain knowledge, two saliency cues are consolidated to generate features maps :

2.3.1 Edge Cue

Edge detection identifies and locates abrupt changes of pixel intensity in MRI which could characterize a discontinuity in the gray matter. We use the Canny edge detector for that task.

2.3.2 Texture Cue

To describe the texture from the MRI images, we resort to the well-known local binary pattern (LBP) descriptor which is proved to be the most used and efficient descriptor to analyze MRI texture for AD diagnosis. LBP comprises a binary code that is obtained by thresholding a neighborhood according to the gray value of its center. Given a center pixel in the image, the LBP value is computed by comparing its gray value with its neighbors. The LBP map of the brain tissue resulting from texture classification reduces the risk of omission and ensures the reproducibility of the diagnosis by drawing the radiologists attention on diagnostically interesting parts.

Texture and edge Features are extracted on multiple scales of the MRI slice and stored in separate feature maps. A unique saliency map is generated through the combination of centre-surround feature maps (conspicuity maps). Finally, a weighted mean of conspicuity maps produces the saliency maps S_{BU}.

2.3.3 Feature Maps Fusion

Finally, the conspicuous maps are fused into a single saliency map as follows:

$$S_{BU} = \frac{1}{2}(Map(LBP) + Map(Edge)) \qquad (6)$$

2.4 Final Saliency Model

The final saliency map is obtained as a fusion of aforementioned top-down and bottom-up maps. The used fusion is a geometric mean between both maps as described below :

$$FS_{AD} = \sqrt{S_{TP}.S_{BU}} \qquad (7)$$

3 RESULTS AND DISCUSSION

3.1 Visual Anatomical Interpretation

With the aim to evaluate the proposed approach, the saliency map is generated using the proposed approach on the MRI of an NC subject. Figure 3 presents the overlaid saliency maps on the MRI slices for this subject. Saliency maps are color-coded according to the relevance of brain regions. For instance, red spots represent the most visually salient (relevant for diagnosis) areas of the MRI. The obtained saliency maps effectively detect and quantify regions of interest that are known to be altered in the degenerative disease and could be more prominent for the clinician attention. In order to consider the difference of saliency maps between AD and NC cases, we compute also saliency maps on the MRI of AD subjects. Saliency maps are illustrated on Figure 4

By mapping the obtained saliency maps, for both NC and AD subjects, with standard anatomical atlas (AAL) (Tzourio-Mazoyer et al., 2002), it is possible to identify the brain areas involved in the discrimination between AD and NC, namely the hippocampus, the parahippocampal gyrus, the entorhinal cortex, and the amygdale. However, when the regions are not yet shrunk (this is the case of NC MRI), clinicians tend to pay more attention to details within the salient regions. This explains the fact that NC saliency maps are different (see slice $s = 85$ and $s = 80$ from Figure 3 and slice $s = 75$ and $s = 80$ from Figure 4) over the corresponding anatomical regions. Another observation concerns the cerebral cortex and temporal lobe (slices 45) that is more salient in the MRI of the AD subjects than NC ones. This indicates that, with the progress in AD, more atrophies are produced. Thus, a small number of brain regions with relatively large atrophies is sufficient for a successful detection of AD. From those saliency maps, we can see that detected regions of interest differ between AD and NC patients depending on the degree of the brain atrophy. Hence, the saliency maps help in discovering meaningful visual patterns witch could be helpful to discriminate AD subjects from NC.

In addition, saliency map shows the ROI preference order (hierarchy) for the diagnosis, hence, the lateral ventricle and the cortex are detected later (less salient). In addition, the saliency maps help to detect the real volume of the hippocampus ROI which constitutes a key step to its effective segmentation.

One would ask about the performance of state-of-the-art saliency models on such a specific problem. To answer this, Figure 5 presents examples of MRI saliency maps generated by our proposed method,

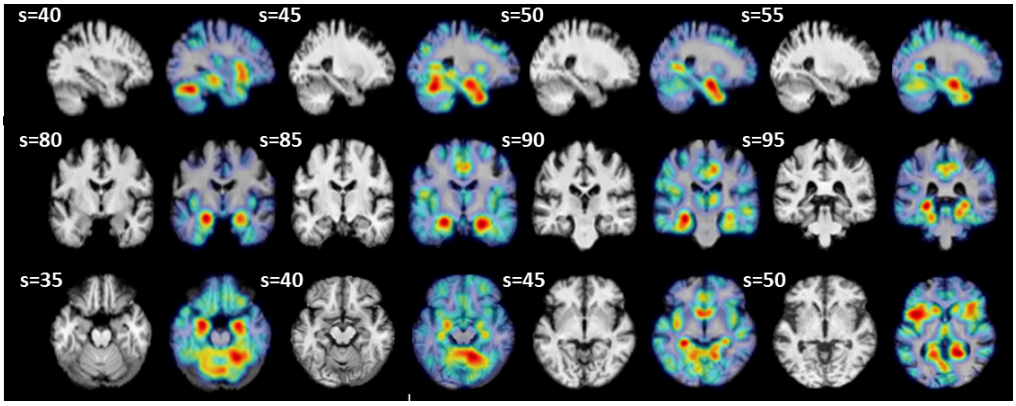

Figure 3: MRI slices selection of NC subject (the subject is 86 years old with an MMSE equal to 30).

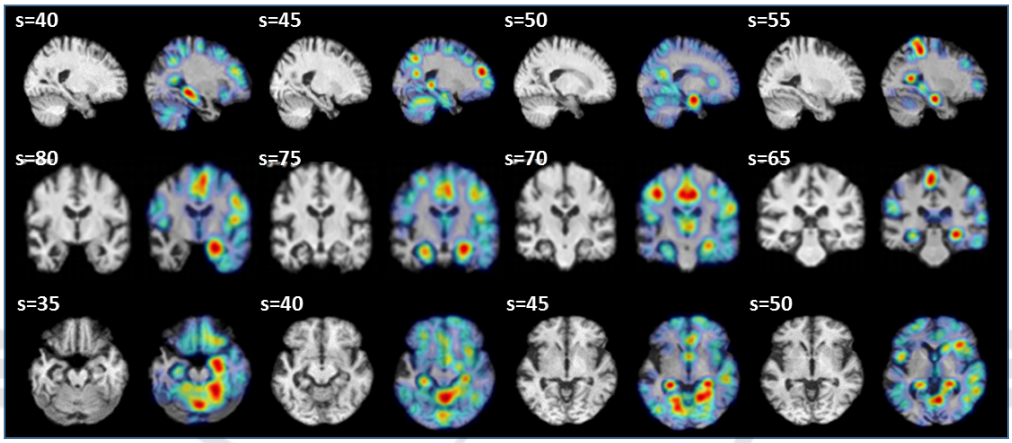

Figure 4: MRI slices selection of AD subject (the subject is 80 years old with an MMSE equal to 25).

and by two famous saliency models namely Itti and GBVS. Those models were proposed for natural scene interpretation. From the illustrated results, it is obvious to notice that both Itti and GBVS algorithms failed to detect relevant regions for Alzheimer's disease compared to our proposed approach. This confirms the role of domain knowledge in improving automatic MRI content analysis and interpretation.

3.2 Subjects Classification

In order to check discrimination capability of our approach, we propose to classify subjects using their saliency maps. An SVM with the histogram intersection kernel (HIK) is used for the classification. The SVM is trained using the normalized saliency maps generated for the subjects in the training set. The diagnostic classification was conducted by selecting a total of 188 subjects from the ADNI database and grouping them into AD, NC and MCI. The AD group contains 66 subjects aged in (76.2 ± 7.4) years with an MMSE ranging in (24.5 ± 0.71). In turn, the NC group contains 54 NC aged in (79 ± 5.3) years with

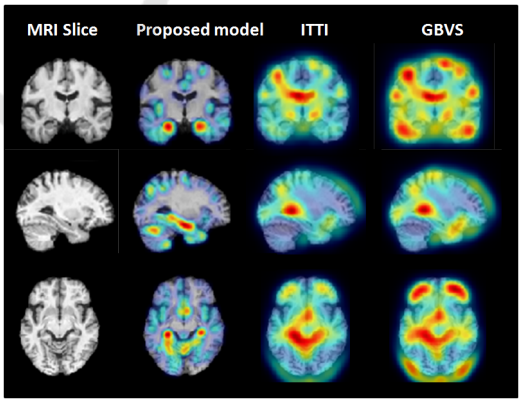

Figure 5: Comparison of the output of our proposed model with regards to two widely used saliency models: Itti and GBVS.

an MMSE ranging in (29.5 ± 1.3). Finally, the MCI group contains 68 NC ranging in (71.2 ± 5.7) years with an MMSE in the mean (27.6 ± 0.5).

Two binary classification problems, AD *vs.* NC and MCI *vs.* NC, have been investigated. To evaluate the performance of different classification methods,

we use 5-fold cross-validation strategy to compute the classification accuracy (for measuring the proportion of subjects correctly classified among the whole population), as well as the sensitivity (i.e., the proportion of AD or MCI patients correctly classified) and the specificity (i.e., the proportion of healthy controls correctly classified). Classification results are presented in Table 1.

Table 1: Diagnostic classification results between AD *vs.* NC and MCI *vs.* NC.

Groups	Accuracy	Sensitivity	Specificity
AD vs NC	81.48 %	83.33%	94.8%
MCI vs NC	76.66%	73.3%	79.82%

For classifying AD from NC, our method achieves a classification accuracy of 81.48%, a sensitivity of 83.33%, and a specificity of 94.8%. On the other hand, for classifying MCI from NC our method achieves a classification accuracy of 76.66%, a sensitivity of 73.3%, and a specificity of 79.82%. Obtained results show that our saliency based atrophy detection approach allows to consistently distinguish subjects with AD or MCI from NC.

4 CONCLUSION

This paper proposed a novel approach for computer-aided diagnosis based on saliency estimation. The proposed framework is based on both bottom-up and top-down subsystems using domain knowledge in AD diagnosis. In the bottom-up approach, information comes from low-level MRI characterization (texture and edge) and the top-down approach includes a learning process to identify and localize the subset of gray matter regions that provide optimal discrimination between groups. The proposed method could help clinicians to evaluate their diagnosis findings. This also makes the diagnosis easier for clinicians with a limited expertise to extract diagnostically useful and objective information. Future work consists in performing clinician's gazes tracking to improve the proposed model with ground truth.

ACKNOWLEDGEMENT

Data collection and sharing for this work was funded by the Alzheimer's Disease Neuroimaging Initiative (ADNI) (National Institutes of Health Grant U01 AG024904). ADNI is funded by the National Institute on Aging, the National Institute of Biomedical Imaging and Bioengineering, and through generous contributions from the following: Abbott; Alzheimer's Association; Alzheimer's Drug Discovery Foundation; Amorfix Life Sciences Ltd.; AstraZeneca; Bayer HealthCare; BioClinica, Inc.; Biogen Idec Inc.; Bristol-Myers Squibb Company; Eisai Inc.; Elan Pharmaceuticals Inc.; Eli Lilly and Company; F. Hoffmann-La Roche Ltd and its affiliated company Genentech, Inc.; GE Healthcare; Innogenetics, N.V.; IXICO Ltd.; Janssen Alzheimer Immunotherapy Research and Development, LLC.; Johnson and Johnson Pharmaceutical Research and Development LLC.; Medpace, Inc.; Merck and Co., Inc.; Meso Scale Diagnostics, LLC.; Novartis Pharmaceuticals Corporation; Pfizer Inc.; Servier; Synarc Inc.; and Takeda Pharmaceutical Company. The Canadian Institutes of Health Research is providing funds to support ADNI clinical sites in Canada. Private sector contributions are facilitated by the Foundation for the National Institutes of Health www.fnih.org. The grantee organization is the Northern California Institute for Research and Education, and the study is coordinated by the Alzheimer's Disease Cooperative Study at the University of California, San Diego. ADNI data are disseminated by the Laboratory for Neuro Imaging at the University of California, Los Angeles. This research was also supported by NIH grants P30 AG010129 and K01 AG030514.

REFERENCES

Agrawal, P., Vatsa, M., and Singh, R. (2014). Saliency based mass detection from screening mammograms. *Signal Processing*, 99:29 – 47.

Ashburner, J. and Friston, K. J. (2000). Voxel-based morphometrythe methods. *Neuroimage*, 11(6):805–821.

Banerjee, S., Mitra, S., Shankar, B. U., and Hayashi, Y. (2016). A novel gbm saliency detection model using multi-channel mri. *PloS one*, 11(1).

Blennow, K., Hampel, H., Weiner, M., and Zetterberg, H. (2010). Cerebrospinal fluid and plasma biomarkers in Alzheimer disease. *Nature Reviews Neurology*, 6(3):131–144.

Braak, H. and Braak, E. (1998). Evolution of neuronal changes in the course of Alzheimer's disease. *Neurology*, 53:127–140.

Chung, A. G., Scharfenberger, C., Khalvati, F., Wong, A., and Haider, M. A. (2015). *Image Analysis and Recognition: 12th International Conference, ICIAR 2015, Niagara Falls, ON, Canada, July 22-24, 2015, Proceedings*, chapter Statistical Textural Distinctiveness in Multi-Parametric Prostate MRI for Suspicious Region Detection, pages 368–376. Springer International Publishing, Cham.

Deepak, K. S., Chakravarty, A., Sivaswamy, J., et al. (2013). Visual saliency based bright lesion detection and discrimination in retinal images. In *Biomedical Imaging*

(ISBI), 2013 IEEE 10th International Symposium on, pages 1436–1439. IEEE.

Fouquier, G., Atif, J., and Bloch, I. (2012). Sequential model-based segmentation and recognition of image structures driven by visual features and spatial relations. *Computer Vision and Image Understanding*, 116(1):146 – 165. Virtual Representations and Modeling of Large-scale Environments (VRML).

Frisoni, G. B., Testa, C., Sabattoli, F., Beltramello, A., Soininen, H., and Laakso, M. P. (2005). Structural correlates of early and late onset Alzheimers disease: voxel based morphometric study. *Journal of Neurology, Neurosurgery and Psychiatry*, 76(1):112–114.

Guyon, I., Weston, J., Barnhill, S., and Vapnik, V. (2002). Gene selection for cancer classification using support vector machines. *Machine learning*, 46(1-3):389–422.

Harel, J., Koch, C., and Perona, P. (2006). Graph-based visual saliency. In *Advances in neural information processing systems*, pages 545–552.

Harper, L., Fumagalli, G. G., Barkhof, F., Scheltens, P., O'Brien, J. T., Bouwman, F., Burton, E. J., Rohrer, J. D., Fox, N. C., Ridgway, G. R., and Schott, J. M. (2016). Mri visual rating scales in the diagnosis of dementia: evaluation in 184 post-mortem confirmed cases. *Brain*.

Hearst, M. A., Dumais, S. T., Osman, E., Platt, J., and Scholkopf, B. (1998). Support vector machines. *Intelligent Systems and their Applications, IEEE*, 13(4):18–28.

Itti, L., Koch, C., Niebur, E., et al. (1998). A model of saliency-based visual attention for rapid scene analysis. *IEEE Transactions on pattern analysis and machine intelligence*, 20(11):1254–1259.

Jampani, V., Sivaswamy, J., Vaidya, V., et al. (2012). Assessment of computational visual attention models on medical images. In *Proceedings of the Eighth Indian Conference on Computer Vision, Graphics and Image Processing*, page 80. ACM.

Lala, D. and Nakazawa, A. (2016). Heat map visualization of multi-slice medical images through correspondence matching of video frames. In *Proceedings of the Ninth Biennial ACM Symposium on Eye Tracking Research & Applications*, ETRA '16, pages 119–122, New York, NY, USA. ACM.

Li, R., Shi, P., and Haake, A. R. (2013). Image understanding from experts' eyes by modeling perceptual skill of diagnostic reasoning processes. In *Computer Vision and Pattern Recognition (CVPR), 2013 IEEE Conference on*, pages 2187–2194.

Ma, L., Wang, W., Zou, S., and Zhang, J. (2009). Liver focus detections based on visual attention model. In *2009 3rd International Conference on Bioinformatics and Biomedical Engineering*, pages 1–5.

Mahapatra, D. and Buhmann, J. M. (2015). *Machine Learning in Medical Imaging: 6th International Workshop, MLMI 2015, Held in Conjunction with MICCAI 2015, Munich, Germany, October 5, 2015, Proceedings*, chapter Visual Saliency Based Active Learning for Prostate MRI Segmentation, pages 9–16. Springer International Publishing, Cham.

Mehmood, I., Baik, R., and Baik, S. W. (2013a). *Automatic Segmentation of Region of Interests in MR Images Using Saliency Information and Active Contours*, pages 537–544. Springer Netherlands, Dordrecht.

Mehmood, I., Ejaz, N., Sajjad, M., and Baik, S. W. (2013b). Prioritization of brain {MRI} volumes using medical image perception model and tumor region segmentation. *Computers in Biology and Medicine*, 43(10):1471 – 1483.

Nodine, C. F. and Kundel, H. L. (1987). Using eye movements to study visual search and to improve tumor detection. *Radiographics*, 7(6):1241–1250.

Pulido, A., Rueda, A., and Romero, E. (2013). Classification of alzheimer's disease using regional saliency maps from brain mr volumes. In *SPIE Medical Imaging*, pages 86700R–86700R. International Society for Optics and Photonics.

Pulidoa, A., Rueda, A., and Romeroa, E. Extracting regional brain patterns for classification of neurodegenerative diseases. In *Proc. of SPIE Vol*, volume 8922, pages 892208–1.

Rueda, A., Gonzalez, F., Romero, E., et al. (2014). Extracting salient brain patterns for imaging-based classification of neurodegenerative diseases. *Medical Imaging, IEEE Transactions on*, 33(6):1262–1274.

Shao, H., Zhang, Y., Xian, M., Cheng, H. D., Xu, F., and Ding, J. (2015). A saliency model for automated tumor detection in breast ultrasound images. In *Image Processing (ICIP), 2015 IEEE International Conference on*, pages 1424–1428.

Tzourio-Mazoyer, N., Landeau, B., Papathanassiou, D., Crivello, F., Etard, O., Delcroix, N., Mazoyer, B., and Joliot, M. (2002). Automated anatomical labeling of activations in {SPM} using a macroscopic anatomical parcellation of the {MNI} {MRI} single-subject brain. *NeuroImage*, 15(1):273 – 289.

Wen, G., Aizenman, A., Drew, T., Wolfe, J. M., Haygood, T. M., and Markey, M. K. (2016). Computational assessment of visual search strategies in volumetric medical images. *Journal of Medical Imaging*, 3(1):015501–015501.

Yuan, Y., Wang, J., Li, B., and Meng, M. Q. H. (2015). Saliency based ulcer detection for wireless capsule endoscopy diagnosis. *IEEE Transactions on Medical Imaging*, 34(10):2046–2057.

Zou, X., Zhao, X., Yang, Y., and Li, N. (2016). Learning-based visual saliency model for detecting diabetic macular edema in retinal image. *Computational Intelligence and Neuroscience*, 2016.